The Casimir Force

a force out of nothing

Abstract

This paper discusses the Casimir force, discovered in 1948. It explains the origin of the Casimir force, and how it can be measured accurately by taking into account finite conductivity, finite temperature and surface roughness. Also its importance for placing constraints on higher dimension theories and its importance in small systems (NEMS) are described.

Marian Otter
MSC
May 31, 2006

Contents

Chapter 1

Motivation

Since I was a child, I have been interested in knowing why things are like they are. So I started reading books, and asking questions. When I grew up, I decided to follow a path in which I could learn to understand the world a little better: I chose the most technical and mathematical direction in highschool and I did my bachelor in applied physics at Rijksuniversiteit Groningen. Here I became familiar with many interesting phenomena, and I started to appreciate the enormous amount of work people all over the world have done to get a better understanding of nature.

Yet our understanding of most phenomena is still incomplete, and much more research is needed. A lot remains a mystery at the moment, and these are the things that intrigue me. One of them, which for first I heard during a lecture of my supervisor, mr. Palasantzas, is the Casimir force. Although it was discovered over 50 years ago, only lately people became aware of the influence this force has in many fields of physics. This makes it a very interesting phenomenon to investigate and to describe. In this paper, I present an introduction to the Casimir force, and its influence in a variety of systems and research field. Before we can reach an complete understanding of this intriguing force and its consequences, we must find a way to do our measurements more accurate. Only then we can prove or invalidate higher dimension theories.

Chapter 2

History and origin

2.1 History

When two mirrors are facing each other in empty space, what will happen? Intuitively, people would say 'nothing', but in fact they will attract each other. This phenomenon was first predicted by the Dutch theoretical physicist Hendrik Casimir in 1948. He was investigating long-range van der Waals forces in colloids together with his collaborator D. Polder. He took the retardation in the electromagnetic intraction of dipoles into account, and arrived at the so called Casimir-Polder forces between polarizable molecules. This was later extended by E.M. Lifshitz to forces between dielectric macroscopic bodies, of which the ideal conductor is a limiting case. The phenomenon first seen by Casimir was named after him the Casimir effect, and the force between the plates is known as the Casimir force. An artist impression is given in figure 2.1.

   The intriguing property of this force is that it is one of only a few existing macroscopic manifestations of quantum phenomena, like superconductivity, superfluidity and the quantum Hall effect. For many years the Casimir force was just a theoretical curiosity. This is because its difficulty to be measured accurately. Nowadays sophisticated equipment has become available, and the Casimir effect can be studied. A new generation of measurements began in 1997 with the experiment of Steve Lamoreaux. He measured the Casimir force between a spherical lens and an optical quartz plate. Both of them were coated with copper and gold. They where connected to a torsion pendulum in vacuum. When the plate and lens where brought together at a few microns, the Casimir force pulled them together and caused the pendulum to twist. Since then, many other researchers tried new Casimir force mea-
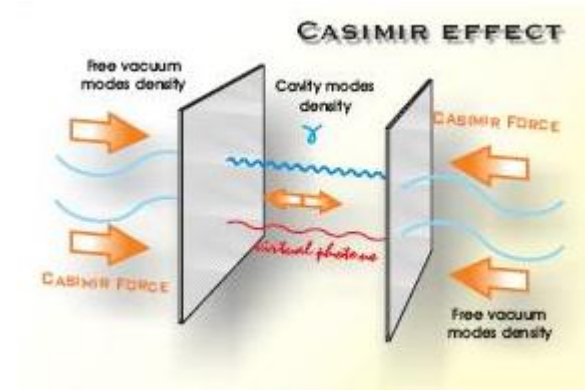
Figure 2.1: An artist view of the Casimir effect. Two flat plane parallel mirrors, which are facing each other in quantum vacuum, are attracted to each other. The Casimir effect is the result of the competition between the intracavity and external vacuum radiation pressure. The intracavity spectral density is modified by the presence of the mirrors with respect to the external one. (Picture taken from [1])

surements. In most cases this is done with a sphere-plate geometry instead of two parallel planes. This is simply because the planes have to be perfectly parallel for the measurement to be succesfull, which is very difficult to realize in practice. The drawback of using the sphere and plane is that the theoretical calculations are not as accurate as for two planes. An overview of the measurements performed lately is given in figure 2.2.

During the last years progress has been made in three different areas. In quantum field theory it is known that when you have flat boundaries the vacuum energy becomes infinite at large momenta in the same way as in free Minkowski space. Therefore, the final physical result for the Casimir energy can be obtained by subtracting the contribution of the Minkowski space, which is the mathematical setting in which Einstein's theory of special relativity is most conveniently formulated. In this setting the three ordinary dimensions of space are combined with a single dimension of time to form a four-dimensional manifold representing spacetime. However, for compact domains bounded by closed surfaces the Casimir energy cannot be obtained in this way. An explicit application to the Casimir effect is for example to relate the known divergencies for the Casimir effect for a massive field with boundary conditions on a sphere to the corresponding heat kernel coefficients. Also the calculation of the Casimir effect for massive fields for nonplane boundaries is understood better now. In condensed matter physics real materials are considered instead of the perfectly smooth plane mirrors

Investigators	Year	Geometry	Method	Distance Scale (nm)	Materials	Pressure (mbar)	Temp (K)	Accuracy (%)
S. K. Lamoreaux	1997		Torsion pendulum	600 - 6000	Au(500nm)	10^{-4}	300	5
U. Mohideen & A. Roy	1998		AFM	100 - 900	Al (300nm) + AuPd (20nm)	5×10^{-1}	300	2
A. Roy and U. Mohideen	1999		AFM	100 - 900	Al (250nm)+ AuPd (8nm)	5×10^{-1}	300	2
G. L. Klimthitskaya, A. Roy, U. Mohideen and V. M. Mostepanenko	1999		AFM	100 - 900	Al (300nm) + AuPd (20nm)	5×10^{-1}	300	1
T. Ederth	2000		Piezo-tube manipulator	20 - 100	$50 \mu m$ Au wires coated in thiol SAM	1000	300	1
H. B. Chan, V. A. Aksyuk, R. N. Kleiman, D. J. Bishop & F. Capasso	2001		MEMS torsion bar capacitance	90 - 1000	Au (200nm) + Cr underlayer	1000	300	1
G. Bressi, G. Carugno, R. Onofrio & G. Ruoso	2002		Interferometry	500 - 3000	Cr (50nm) on Si	10^{-3}	300	15
R. S. Decca, D. Lopez, E. Fischbach & D. E. Krause	2003		MEMS torsion bar capacitance	200 - 2000	Cu/Au	10^{-4}	300	1
NANOCASE	2005-		AFM, MEMS	10 - 1000	Si, Au	10^{-11}	20 - 1000	<1

Figure 2.2: An overview of the latest measurements with some information about the experiment. The claimed accuracy is still under debate.

that Hendrik Casimir based his theory on. For real materials some problems
arise. The first one is that not all frequencies are reflected perfectly. This
problem was already tackled by Lifshitz in the mid-1950's. Another problem
is the temperature. Casimir set the temperature to zero. When this is not
the case, as it is usually in experiments, thermal and vacuum fluctuations
come into play. Together they can produce their own radiation pressure and
create a bigger Casimir force than expected. These thermal fluctuations are
only important at length scales larger than 1 μm, while at shorter separa-
tions the wavelength of the fluctuations is too big to fit inside the cavity.
Another problem is that real mirrors have surface roughness. In addition,
the conductivity of the boundary metal is finite. All these factors should be
included in realistic calculations. This can only be done if both the influ-
ence of each individual factor and their combined action can be investigated
experimentally. This has been done lately. The third development concerns
more precise measurements of the Casimir force between metallic surfaces.
As a result calculations of the constraints on hypothetical forces are possible,
e.g. ones predicted by supersymmetry, supergravity and string theory.

2.2 Origin

The Casimir effect is the interaction of a pair of neutral, conductive, parallel
planes due to the disturbance of the vacuum of the electromagnetic field.
In classical electrodynamics there is no force between two neutral plates,
so the effect is a pure quantum effect. Only the vacuum (the ground state
of quantum electrodynamics, QED) causes the plates to attract each other
and leads to a macroscopic quantum effect. In this section, we follow the
article of Bordag, Mohideen and Mostepanenko [2] to explain the origin of
this force.
    The roots of the Casimir effect date back to the introduction of the half-
quanta by Planck in 1911. In the language of quantum mechanics one has
to consider a harmonic oscillator with energy levels $E_n = \hbar\omega(n + \frac{1}{2})$, where
$n = 0, 1, ...$, and $\hbar$ is the Planck constant. It is the energy

$$E_0 = \frac{\hbar\omega}{2} \tag{2.1}$$

of the ground state ($n = 0$) which matters here. This ground state energy
cannot be observed by measurements within the quantum systen, i.e. in
transitions between different quantum states, or for instance in scattering
experiments. However, the frequency ω of the oscillator may depend on
parameters external to the quantum system.

In quantum field theory there is the problem of ultraviolet divergencies which come into play when one tries to assign a ground state energy to each mode of the field. One has to consider then

$$E_0 = \frac{\hbar}{2} \sum_J \omega_J \tag{2.2}$$

where the index J labels the quantum numbers of the field modes. For instance, for the electromagnetic field in Minkowski space the modes are labeled by a three vector $\mathbf{k}$ in addition to the two polarizations. The sum in equation 2.2 is clearly infinite. Casimir was the first to extract the finite force acting between the two parallel neutral plates

$$F_a = -\frac{\pi^2}{240} \frac{\hbar c}{a^4} S \tag{2.3}$$

from the infinite zero-point energy of the quantized electromagnetic field confined in between the plates. Here a is the separation between the plates, $S >> a^2$ is their area, and c is the speed of light. To do this Casimir had subtracted away from the infinite vacuum energy of eqn. 2.2 in the presence of plates, the infinite vacuum energy of quantized electromagnetic field in free Minkowski space. Both infinite quantities were regularized and after subtraction, the regularization was removed leaving the finite result. In the standard textbooks on quantum field theory the dropping of the infinite vacuum energy of free Minkowski space is motivated by the fact that energy is generally defined up to an additive constant. Thus, it is suggested that all physical energies be measured starting from the top of this infinite vacuum energy in free space. In this way effectively the infinite energy of free space is set to zero. This is mathematically done by the normal ordering procedure. However, this procedure cannot be applied when there are external fields or boundary conditions, e.g. on the parallel metallic plates placed in vacuum.

Most experiments are done by measuring the Casimir force between a sphere and a plate to avoid problems of parallelism. Since no exact result is available for this geometry, an approximation should be made. In the 1930's, it was recognized that if the separation between the sphere and the plate is very small compared to the radius of curvature of the sphere, the latter force may be derived from the energy for the parallel plate configuration. This is usually called the Proximity Force Approximation (PFA) or the Proximity Force Theorem. This approximation amounts to summing up the force contributions corresponding to the various inter-plate distances as if these contributions were independent and additive, which is in general not

the case. Within the PFA,

$$F_a = 2\pi R\epsilon(a) = -\frac{\pi^3}{360}\frac{R}{a}\frac{\hbar c}{a^2}S \qquad (2.4)$$

in which d is the distance of closest approach between the plate and the sphere, and R is the radius of the sphere. This follows from

$$
\begin{aligned}
V_a &= \int_0^\pi 2\pi R\sin(\theta)Ra\theta\epsilon(a + R(1 - \cos(\theta))) \\
&= 2\pi R\int_{-R}^R dx\epsilon(a + R - x) \qquad (2.5)
\end{aligned}
$$

and

$$
\begin{aligned}
F_a &= -\frac{\delta V}{\delta a} \\
&= 2\pi R\int_{-R}^R dx\frac{\delta}{\delta x}\epsilon(a + R - x) \\
&= 2\pi R[\epsilon(a) - \epsilon(a + 2R)] \\
&\approx 2\pi R\epsilon(a) \quad \text{if } a << R \qquad (2.6)
\end{aligned}
$$

Now because $\epsilon_a = -\frac{\pi^2}{720a^3}$, the result for F follows.

2.3   Atom-atom interactions

The nature of atom-atom interactions is a fundamental conceptual issue which needs both physics and chemistry to be described. These interactions are for example important to understand the stability of matter. The energy of interaction between two neutral atoms can be determined by using perturbation methods, which was originally done by Casimir [3]. He was investigating colloidal solutions with his collegue Polder and realized that their behaviour could only be described when a retardation of the van der Waals force was taken into account. This led to the discovery of the Casimir force.

The unperturbed states of the system (consisting of two atoms and the radiation field) are assumed to be the states that are completely defined by the states of the two atoms and the state of the radiation field in empty space. The perturbation operator, which is responsible for the interaction of the two atoms, contains the electrostatic interaction Q between the charged particles of the first atom with those of the second atom, the interaction

G_A between the first atom and the radiation field, and the interaction G_B between the second atom and the radiation field.

Now with the aid of the perturbation operator $G_A + G_B + Q$ the energy perturbation is determined by using up to fourth order perturbation theory. The total result of the calculation is divergent, but the terms that depend on the distance R between two atoms have a finite value, which is the total energy of interaction between the two atoms. It turns out that there are three different kind of terms in the total expression:

1. Terms obtained by applying second-order perturbation theory with the electrostatic interaction are proportional to e^2 where e is the electronic charge. The result is equal to the usual expression for the London energy.

2. Terms obtained by applying third-order perturbation theory are restricted to the terms that contain Q.

3. Terms obtained by determining the energy perturbation with the aid of the operator $G_A + G_B$, the electrostatic interaction now being omitted.

All the results are proportional to e^4. Calculating all these terms using the Heisenberg method, which states that even when the quantities of the electromagnetic field are considered as matrices, they satisfy Maxwell's equations, and collecting terms gives an expression which can be simplified because a number of terms cancels. The result is

$$V(R) = -\frac{23}{4\pi}\hbar c\frac{\alpha^2(0)}{R^7} \tag{2.7}$$

where $\alpha(0)$ is the static polarizability of the (identical) atoms and c is speed of light. The formula only holds under the condition $R >> c/\omega_0$ where ω_0 is the principle absorption frequency of the atoms. The full calculation can be found in Casimir's original paper [3].

Equation 2.7 contains the speed of light c, because of which it has been iterpreted as a retardation effect due to the finite velocity of the photons mediating the interaction. The idea is that the potential is softened when the distance is sufficiently large for the finite value of the speed of light to induce a significant loss of interatomic correlations in the dipole fluctuations. For small distances this is not the case, and London showed that the correct formula for the attractive disperion force equal is to

$$V(R) = -\frac{3}{4}\hbar\omega_0\frac{\alpha^2(0)}{R^6}. \tag{2.8}$$

Since then, these two formulas have been used extensively in calculations in different context, such as the theories of dilute gasses, colloidal stability and atomic spectroscopy.

These equations are valid at T = 0 K. When the temperature is finite, the equation for separations $R >> \hbar c / k_B T$ should be modified to the form

$$V(R, T) = -3 k_B T \frac{\alpha^2(0)}{R^6}.$$ (2.9)

This was shown by Wennerström [4]. Frequently one presents the total interaction between macroscopic bodies at finite temperature in terms of a sum of a 'zero-frequency classical' term and a 'quantum' term involving a sum over all other frequencies. Equation 2.8 arises form the 'zero-frequency classical' term. It is tempting to think that this asymptotic form is present at all separations and only dominant when all other terms have decayed away. The reality is more subtle, because the 'classical zero-frequency' term is, in fact, exactly cancelled by a contribution arising from the 'quantum' terms. The temperature correction suggests that the weakening of the potential is due to the quantum nature of light, and that at large separations and finite temperatures there is no dependence on c. More investigations have to be performed before this explanation can be confirmed.

2.4   Role of the Casimir force in different fields of physics

The Casimir effect plays an important role in a variety of fields of physics such as quantum field theory, condensed matter physics, atomic and molecular physics, gravitation, cosmology and mathematical physics. Below the most important applications of the different fields according to Bordag, Mohideen and Mostepanenko [2] will be summed.

In quantum field theory there are three main applications. In the bag model of hadrons in quantum chromodynamics the Casimir energy of quarks and gluon fields makes essential contributions to the total nucleon energy. In Kaluza-Klein field theories it is because of the Casimir effect that extra spatial dimensions can compactify spontaneously. Furthermore, measurements of the Casimir force provide opportunities to obtain stronger constraints for the parameters of long-range interactions and light elementary particles predicted by the unified gauge theories, supersymmetry, supergravity and string theory. Also, by measuring the Casimir force, Newton's inverse-square

law of gravitation can be tested accurately for the first time at length scales below 1 μm.

In condensed matter physics, the Casimir effect leads to attractive forces between closely spaced material boundaries, which depend on the configuration geometry, temperature, and the electrical and mechanical properties of the boundary surface. It is responsible for some properties of thin films, and should be taken into account in investigations of surface tension and latent heat. The Casimir effect plays an important role in both bulk and surface critical phenomena.

In gravitation, astrophysics, and cosmology, the Casimir effect arises in space-time with nontrivial topology. The vacuum polarization resulting from the Casimir effect can drive the inflation process. In the theory of structure formation of the universe due to topological effects, the Casimir vacuum polarization near the cosmic strings may play an important role.

In atomic physics the long-range Casimir interaction leads to corrections to the energy levels of Rydberg states. In quantum electrodynamics a number of Casimir-type effects arise when the radiative processes and associated energy shifts are modified by the presence of the cavity walls.

In mathematical physics the investigation of the Casimir effect has stimulated the development of powerful regularization and renormalization techniques based on the use of zeta functions and heat kernel expansion.

For a long time it was thougt that the Casimir force in some situations could be repulsive instead of attractive. But in a recent theoretical study Hertzberg [5] showed that this is due to the neglectance of cutoff during Casimir force calculations for real materials. When this is taken into account, the force changes from repulsive to attractive. Hertzberg considers a 3-dimensional piston, for both scalar and electromagnetic fields. This is a modification of the usual rectangle for which the cutoff dependences cancel. Both pistons of rectangular and arbitrary cross sections are considered. He shows that the force on the piston is always attractive for a rectangular cross section and gives arguments why this should be true for any cross section. From this it follows that in any physically realizable system the force should be attractive.

This paper gives an overview of interesting aspects of the Casimir force. It is not intended to be complete, nor will go into difficult mathematics. In the reference articles can be found the complete derivation of the Casimir force, and some of the applications. The next chapters are organized as follows: chapter 3 will give an overview of the Casimir force measurements. The idea here is to give an example of different types of measurement and of different geometries. Chapter 4 describes the consequences the Casimir

force has for our understanding of fundamental forces. What it called the fifth force and which are the consequences for the models about higher dimensionality? Chapter 5 is about nano electromechanical systems (NEMS) and micro electromechanical systems (MEMS) and the role of the Casimir force in the working of these systems. Finally, chapter 7 will focus on future prospects.

Chapter 3

Measurements

3.1 General requirements for Casimir force measurements

The benchmarks for measuring the Casimir force were set by Sparnaay, who did the first experiments on this phenomenon. The experimental techique was based on a spring balance and parallel plates. The requirement from the instrumental point of view are the extremely high force sensitivity and the capability to reproducibly measure the surface separation between two surfaces. Sparnaay [6] gives, according to [2] the following requirements:

1. clean plate surfaces completely free of chemical impurities and dust particles;

2. precise and reproducible measurement of the separation between the two surfaces which is nonzero due to the roughness of the metal surfaces and the presence of dust;

3. low electrostatic charges on the surface and low potential differences between the surfaces. There can exist a large potential difference between clean and grounded metallic surfaces due to the workfunction differences of the materials used, and the cables used to ground the metal surfaces. Thus an independent measurement of the systematic error due to the residual electrostatic force is absolutely necessary.

These requirements are difficult to obtain in practice and even more difficult to obtain together. Often, one or more of the above were neglected in the force measurements. Other things that are nessecary to take into account in a proper manner are surface roughness, temperature effects, and finite

conductivity corrections. First it was assumed that each correction factor independently influences the Casimir force, so there are no multiplicative effects. Now it is understood that it is not that simple. Lambrecht *et al.* [7] showed that the corrections for the finite temperature on one hand and the finite conductivity on the other hand are important at different length scales. The influence of temperature is important for $a > \lambda_T = \frac{2\pi c}{\omega_T} = \frac{\hbar c}{k_b T}$. λ_T is approximately 7μm at room temperature. At smaller distances it is a constant factor. In contrast, the finity conductivity of metals has an appreciable effect for distances smaller than or of the order of the plasma wavelength $\lambda_P = \frac{2\pi c}{\omega_P}$ which is approximately $0.1 - 0.2\mu$m. At higher distances, it is a constant factor. This can be seen in fig. 3.1 Now it is known that the surface
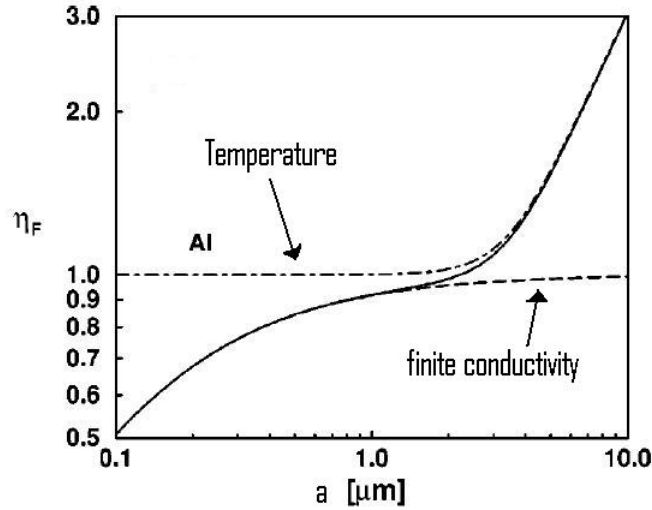
Figure 3.1: Force correction factor for Al as a function of the mirrors distance at $T = 300K$. $\eta_F = F/F_{Cas}$ is the corrected Casimir force divided by the ideal Casimir force. (Picture taken from [7]).

roughness is active at the same length scales as the finite conductivity. This means that we can calculate the total correction to the Casimir force by first summing the contributions of finity conductivity and surface roughness and then multiplying it with the contribution for the finite temperature. However, this receipt for the different corrections to the Casimir force only holds when an accuracy of less than 1% is required. To obtain a higher accuracy more sophisticated methods to account for their combined effect are needed. Below the different factors will be discussed separately.

3.2   Surface roughness

Bezerra [8] showed that the Casimir force is increased by the surface roughness in terms of a relation for the Casimir energy

$$E_{pp,r} \approx E_{pp} \left(1 + 6 \frac{w^2}{a^2} \right) \tag{3.1}$$

in which w is the rms roughness amplitude and a is the distance between the two plates. For a periodically rough plate (wavelength Δ and amplitude A_r), the Casimir energy is given by the simple analytic asymptotic expressions

$$E_{pps} \approx E_{pp} \begin{cases} 1 + 3(A_r^2/\Delta^2) & \text{if } \Delta >> a \\ 1 + 2\pi(A_r^2/\Delta a) & \text{if } \Delta << a \end{cases} \tag{3.2}$$

When the short wavelength roughness also plays a role, besides the rms roughness amplitude w and the latereal correlation length ξ, as is the case for a random self-affine rough plate (which is commonly observed after deposition of metal films on plates) things become much more complicated. How this situation can be described mathematically is still under investigation. For plates in NEMS and MEMS, which are made by coating a substrate with a thin metal film using e.g. the sputtering technique or electron beam evaporation, the roughness of the metal coating will generally evolve with film thickness in a manner that depends on preparation conditions. Therefore, the way the dynamic evolution of the plate roughness can influence the roughness contribution on the Casimir energy must also be considered.

Recently, the roughness correction to the Casimir force was calculated by Neto, Lambrecht and Reynaud [9]. It was done by a perturbative method to second order for two parallel plate mirrors but can also be applied to the plate sphere geometry. The correction is calculated without using the proximity force approximation, which is obtained as a limiting case for very smooth surfaces.

This correction of [9] is valid within the weak roughness approximation, for which $\rho_{rms} = [< |\nabla h|^2 >]^{1/2} << 1$ is the average local slope. ρ_{rms} is given in the form

$$\rho_{rms} = [\int_0^{Q_c} q^2 \frac{< |h(q)|^2 >}{2\pi^2} d^2 q]^{1/2}. \tag{3.3}$$

$Q_c = \pi/a_0$ with a_0 an atomic size lower cut-off.

Assuming single valued roughness fluctuations $h(R)$ of the in-plane positions $R = (x, y)$ and the same roughness for both plates, the Casimir energy

is given by

$$E_{ca} \cong E_{cf} + \frac{1}{2} \left(\frac{\delta^2 E_{cf}}{\delta a^2} \right) \left[2 \int \frac{d^2 q}{(2\pi)^2} P(q) < |h(q)|^2 > \right] \qquad (3.4)$$

with $E_{cf} = -(\pi^2 hc/720a^3) A_f$ the Casimir energy for a flat perfectly conducting surface, and $< |h(q)|^2 >$ the roughness spectra ($< h >= 0$). A_f is the average flat plate surface area. Taking into account the finite plasmon wavelength λ_p of metals, the scattering function $P(q)$ is given by the simpified expressions

$$P(q) = \begin{cases} \text{if } a < \lambda_p : 0.4492aq & \text{for } q >> 2\pi/a, q >> 2\pi/\lambda_p \\ \text{if } a > \lambda_p : \frac{1}{3}aq & \text{for } 2\pi/a << q << 2\pi/\lambda_p \\ \text{if } a > \lambda_p : \frac{7\lambda_p}{15\pi}q & \text{for } q >> 2\pi/a, q >> 2\pi/\lambda_p \end{cases} \qquad (3.5)$$

This equation is derived under the assumption that the optical response of the metallic plates is described by a plasma model with a dielectric function $\epsilon(\omega) = 1 - (\omega_p/\omega)^2$ where ω_p is the plasma frequency. Finally, upon substitution of this equation in equation 3.4 the Casimir force is obtained:

$$F_{ca} = -\frac{dE_{ca}}{da} \cong F_{cf} \left(1 + \frac{2C_a}{a} \right), \qquad (3.6)$$

$$C_a = \begin{cases} 0.4492 \int_{Q_a}^{Q_c} q < |h(q)|^2 > \frac{d^2 q}{(2\pi)^2} & \text{if } a < \lambda_p \\ \frac{1}{3} \int_{Q_a}^{Q_{\lambda_p}} q < |h(q)|^2 > \frac{d^2 q}{(2\pi)^2} + \frac{7\lambda_p}{15\pi a} \int_{Q_{\lambda_p}}^{Q_c} q < |h(q)|^2 > \frac{d^2 q}{(2\pi)^2} & \text{if } a > \lambda_p \end{cases}$$

Here $Q_{\lambda_p} = 2\pi/\lambda_p$ and $Q_a = 2\pi/\lambda_a$.

3.3   Temperature

When real mirrors are characterized by frequency dependent reflection coefficients, the Casimir force is obtained as an integral over frequencies and wavevectors associated with vacuum and thermal fluctuations. The Casimir force consists of two parts, one for each field polarization. They have the

same form in terms of the corresponding reflection coefficients [7]

$$F = \sum_{-\infty}^{\infty} \frac{\omega_T}{2} F\left[k\omega_T\right], \tag{3.7}$$

$$\mathrm{F}\left[\omega \geq 0\right] = \frac{\hbar A}{2\pi^2} \int_{\frac{\omega}{c}}^{+\infty} d\kappa\kappa^2 f,$$

$$f = \frac{r_\perp^2\left(i\omega, i\kappa\right)}{e^{2\kappa a} - r_\perp^2\left(i\omega, i\kappa\right)} + \frac{r_{ll}^2(i\omega, i\kappa)}{e^{2\kappa a} - r_{ll}^2(i\omega, i\kappa)},$$

$$\mathrm{F}\left[-\omega\right] = \mathrm{F}\left[\omega\right].$$

$r_\perp$ (r_{ll}) denotes the amplitude reflection coefficient for the orthogonal (parallel) polarization of one of the two mirrors, which are supposed to be identical. a is the distance of closest approach of the two plates, ω is the frequency and κ is the wavevector along the longitudinal direction of the cavity formed by the two mirrors. The Casimir force may also be written as a Fourier transform

$$F = \sum_{m=-\infty}^{\infty} \tilde{F}(m\lambda_T), \tag{3.8}$$

$$\tilde{F}(x) = \int_0^\infty d\omega \cos\left(\frac{\omega x}{c}\right) \mathrm{F}\left[\omega\right].$$

The contribution of vacuum fluctuations corresponds to the contribution $m = 0$ in equation 3.9, which is

$$\tilde{F}(0) = \int_0^\infty d\omega \mathrm{F}\left[\omega\right]. \tag{3.9}$$

Hence, the whole force 3.9 is the sum of this vacuum contribution and of thermal contributions $m \neq 0$. The metallic mirrors are described by the plasma model, $\epsilon(\omega) = 1 - (\omega_P^2\omega)^2$ with ω_P the plasma frequency. In this model, the reflection coefficients are given by

$$r_\perp = -\frac{\sqrt{\omega_P^2 + c^2\kappa^2} - c\kappa}{\sqrt{\omega_P^2 + c^2\kappa^2} + c\kappa}, \tag{3.10}$$

$$r_{ll} = \frac{\sqrt{\omega_P^2 + c^2\kappa^2} - c\kappa(1 + \omega_P^2/\omega^2)}{\sqrt{\omega_P^2 + c^2\kappa^2} + c\kappa(1 + \omega_P^2/\omega^2)}.$$

When $c\kappa \leq \omega_P$, which is to say that the distance $a >> \lambda_P$, the Casimir force entails the ideal expression. The Casimir energy is obtained by integration

$$E = \int_L^\infty F(x)dx. \tag{3.11}$$

When this is done at constant temperature, the energy obtained corresponds to the thermodynamical definition of a free energy. The whole correction of energy due to conductivity and temperature effects with respect to the ideal Casimir energy is the factor $\eta_E = E/E_{Cas}$. It is positive, which means that the Casimir energy is a binding energy and the force is attractive. The corrected force can be obtained by multiplying the ideal Casimir force with the factor [11]

$$F_T(T) = 1 + \frac{720}{\pi^2}g(n) \tag{3.12}$$

where

$$g(n) \approx \begin{cases} \frac{n^3}{2\pi}\zeta(3) - \frac{n^4\pi^2}{45} & \text{for } n \leq \frac{1}{2} \\ \frac{n}{8\pi}\zeta(3) - \frac{\pi^2}{720} & \text{for } n > \frac{1}{2} \end{cases}$$

with $n = \frac{2\pi k_b T}{hc}a$ and $\zeta(3) \approx 1.2002$ the Riemann zeta function.

At room temperature we have $n = 0.13 \times 10^{-3}a/nm$. For surface separation $a < 1000$ nm the temperature correction is much less than 1%. This is because for smaller separations the wavelength of the fluctuation is too big to fit inside the cavity for both parallel plate and plate sphere configurations.

3.4 Finite conductivity

Finite conductivity is caused by the fact that real materials become transparant for electromagnetic waves of frequency $\omega < \omega_p$, where ω_p is the plasma frequency. For such high frequency there are no boundary conditions, which means that their mode density is equal everywhere in space. This decreases the difference in the number of modes inside and outside the volume included between the two bodies. The actual strength of the Casimir force will thus be lower than theoretically predicted. The finite conductivity correction, based on the free electron model of the reflectivity of metals, to second order for a given metal with plasma frequency ω_p is given by the factor [12]

$$F_c(\omega_p) = 1 - 4\frac{c}{d\omega_p} + \frac{72}{5}\left(\frac{c}{d\omega_p}\right)^2. \tag{3.13}$$

3.5   Parallel plates measurements

As mentioned before, parallel plate measurements are quite difficult because perfect alignment of the plates is needed. The first measurement of this geometry was done by Bressi *et al.* [13] in the $0.5 - 3\mu m$ range and at a 15 % precision level. There has been one attempt before of Sparnaay, but large systematic errors and uncontrollable electrostatic forces prevented a detailed quantitative study. In the experiment of Bressi *et al.*, the two parallel surfaces are the opposing faces of a cantilever beam, free to oscillate around its clamping point, and of another thicker beam rigidly connected to a frame with adjustable distance from the cantilever. This is shown in figure 3.2. A rectangularly shaped cantilever made of silicon is used with optically
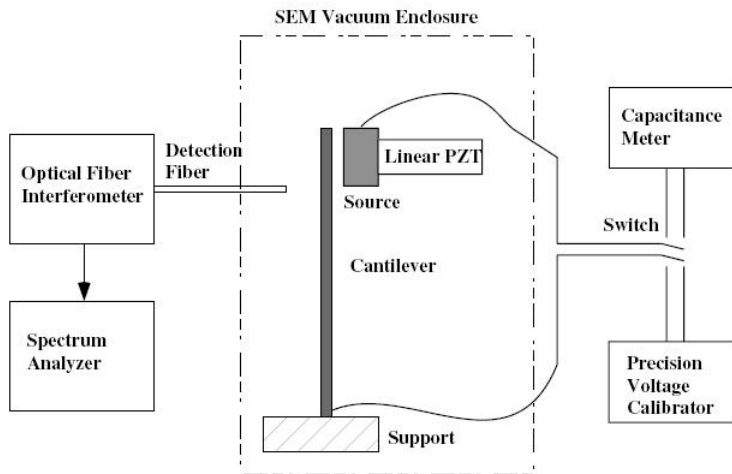
Figure 3.2: Experimental setup. From left to right: displacement transducer, cantilever, and opposing surface (source) solidal to a PZT actuator, capacitance meter, and precision voltage source. The two opposing surfaces, on which the Casimir force is studied, form a capacitor with an area of $1.2 \times 1.2 mm^2$. The source, the PZT, its support, and the motors are mechanically decoupled from the resonator by means of a set of alternated rubber rings and stainless steel disks. The apparatus is placed on the flange accessing the science chamber of a scanning electron microscope (SEM). (This and next picture taken from [13]).

flat surfaces, covered with a 50 nm thick chromium layer. The resonator is
clamped to a copper base by which it can be rotated around the horizontal
axis, parallel to its faces, by using a nanometer step motor. The resonator
is faced on one side by another silicon beam (the source), placed along the
orthogonal direction and also covered by a (thicker) chromium layer. This
beam has the same longitudinal dimensions as the first one but is much
thicker. The source beam can be rotated by using step motors around the
two axes complementary to the one controlled by the resonator tilting, thus
providing fine control of the parallelism of the two opposing surfaces. The
gap separation betweem the two surfaces is adjusted with a dc motor for the
coarse movement, and finely tuned using a linear piezoelectric transducer
ceramic attached to the source. The source and the resonator are electri-
cally connected to a voltage calibrator for the electrostatic calibrations or,
alternatively, to an AC bridge for measuring the capicitance of the system.
A fiber optic interferometer is used to detect the motion of the resonator.
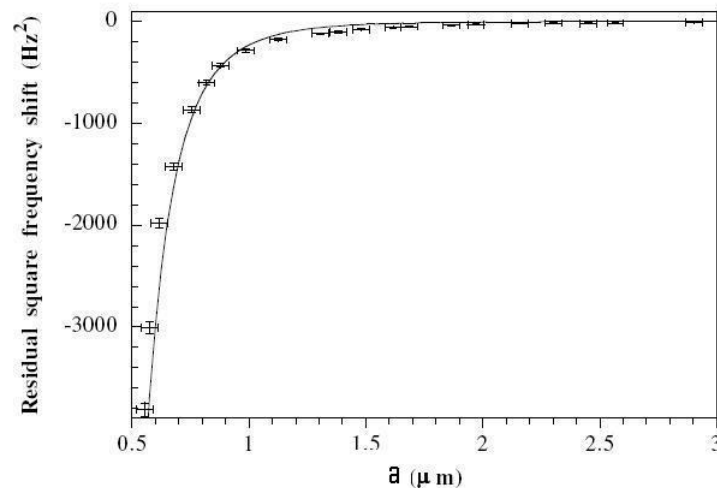
Figure 3.3: Observation of the Casimir force. Residuals of the square fre-
quency shift versus the gap distance.

The problem of parallellism is overcome by first going to an almost par-
allel configuration by means of the various motion controls and obtain the
final parallelism using an AC bridge by maximizing the capacitance at the
minimum obtainable gap separation. In this way a parallelism better than
30 nm over 1.2 mm is reached. To control deviations from electrical neutral-
ity of the two surfaces and determine the offset voltage V_0, which is always

present, the static deflection of the resonator versus the external voltage V_c applied with the calibrator for various gap distances is measured. The bending is measured by looking at the DC level of the fiber optic interferometer signal and a repetitive procedure is adopted to cancel out the effect of drifts in the laser frequencies. The result is a measurement of $\Delta\nu^2(a) = -C_{cas}/a^5$ within 15% precision, as is shown in figure 3.3. Here $\Delta\nu(a)$ is the frequency shift, a is the distance between the plates, and $C_{cas} = K_C S/\pi^2 m_{eff}$ with S the effective area delimited by the cantilever and the source surfaces, m_{eff} the effective mass of the resonator mode, and K_C a constant.

More measurements of the Casimir force between two parallel plates are done, for example, by Chan [14], which determines the influence of the Casimir effect on the oscillatory behavior of microstructures. Genet [7] did theoretical calculations for plane metallic mirrors at nonzero temperature. Temperature and conductivity effects are treated simultaneously, which leads to a temperature dependent function that allows simple estimations that are accurate below the 1% level.

3.6 Plate - sphere measurements

Because measurements between a sphere and a plate are much easier to realize than between two parallel plates, this kind of measurements has been done copiously. In this section I will describe one representative series of measurements in detail and give some references to other measurements.

Mohideen *et al.* [2] used the increased sensitivity of the Atomic Force Microscope (AFM) to do measurements on the Casimir force. Using this method, they report a statistical precision of 1% at smallest separations in their measurements of the Casimir force. A schematic diagram of the experiment is shown in figure 3.4. When there is a force between the sphere and the plate, the cantilever will flex. This flexing is detected by the deflection of the laser beam leading to a difference signal between photodiodes A and B. The difference signal of the photodiodes can be calibrated by means of an electrostatic force. The sphere consists of polystyrene, has a diameter of $200 \pm 4\mu$m and is mounted on the tip of the metal coated cantilevers with Ag epoxy. A sapphire disc of 1 cm diameter which is optically polished is used as a plate. The cantilever, sphere and plate are coated with about 300 nm of aluminum by thermal evaporation. Aluminum coatings are easy to apply due to the strong adhesion of the metal to a variety of surfaces and its low melting point.

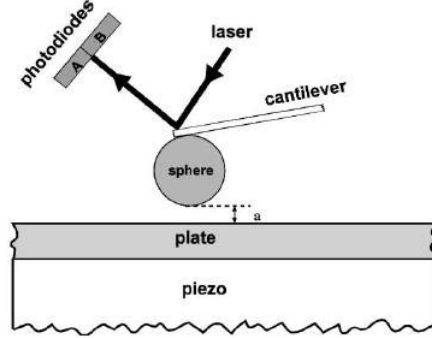The sphere and plane are grounded together with the AFM. The plate

Figure 3.4: Schematic diagram of the experimental setup. Application of a voltage to the piezo electric element results in the movement of the plate towards the sphere. (This and next two pictures taken from [2]).

is then moved towards the sphere in steps while the photodiode difference signal is measured. Next, the force constant of the cantilever is calibrated by an electrostatic measurement. Now different voltages in the range $\pm 0.5V$ to $\pm 3V$ are applied to the plate. The force between the charged sphere and plate is then given by

$$F = \frac{1}{2}(V_1 - V_2)^2 \sum_{n=1}^{\infty} \operatorname{csch}(n\alpha) \left[\coth(\alpha) - n \coth(n\alpha)\right] \qquad (3.14)$$

Here V_1 is the applied voltage on the plate and V_2 represents the residual potential on the grounded sphere. Furthermore, $\alpha = \cosh^{-1}(1 + a/R)$, where R is the radius of the sphere and a is the separation between the sphere and the plate. The systematic error corrections due to the residual potential on the sphere and the true separations between the two surfaces are calculated and taken into account. The result for large distances is shown in figure 3.5 and the result for smaller distances in figure 3.6.

In this experiment, corrections are estimated for the roughness of the surfaces, which can be measured with the AFM directly, and the finity conductivity. The finite temperature corrections are negligibly small for these separation distances.

The following year, Mohideen *et al.* [2] performed an improved version of this experiment; the metal coatings were made smoother, which reduces the effect of surface roughness and allows for smaller separations between the two surfaces, vibration isolations reduced the total noise, independent
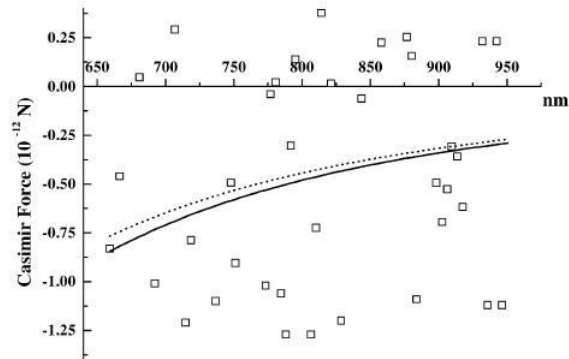
Figure 3.5: Measured average Casimir force for large distances as a function of the plate-sphere separation is shown as open squares. The theoreticial Casimir force with corrections to surface roughness and finite conductivity is shown by the solid line (when the space separation is defined as the distance between Al layers) and by the dashed line (with the distance between Au/Pd layers).

electrostatic measurements of the surface separations were done and the systematic errors were reduced. The average precision level remained at 1%. The only problem was that the use of aluminum surfaces required a thin Au/Pd coating on top. This coating could only be treated in a phenomenological manner, because a more complete theoretical treatment is too complicated.

The next experiment was done with gold surfaces. In this way the Au/Pd coating as on top of the aluminum surface can be avoided, because Au is an inert metal. Again finite temperature corrections are so small that they can be neglected. Because the AFM cantilevers must have a good conductivity, they are coated with aluminum. Therefore, because of the potential difference between aluminum and gold, special care has to be taken in making the electrical contacts to avoid the development of contact potential differences between the plate and the sphere. The systematic error is reduced to 0.1% of the Casimir force at closest separation in this experiment. Now the precision is even better than the 1% of the experiments done before.

Before Mohideen et al. did this series of measurements, a landmark experiment was done by Lamoreaux [15]. He managed to measure the Casimir force in the range $0.6 - 6\mu$m. Because of this measurement both the theoretical and experimental community became aware of the usefulness of the Casimir force measurements to test the forces in the submillimeter range.
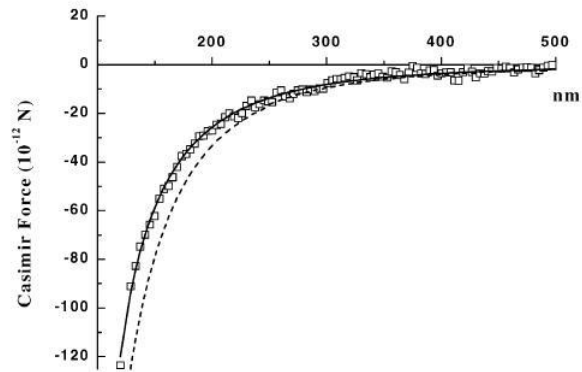
Figure 3.6: Measured average Casimir force for small distances as a function of plate-sphere separation is shown as open squares. The theoretical Casimir force with corrections due to the surface roughness and finite conductivity is shown by the solid line, and without any corrections by the dashed line.

Furthermore, it was the first time that the parameters that are needed for a careful calculation of the experimental precision were measured and reported.

Ederth [16] has investigated which materials are suitable for direct force measurements of the Casimir force between macroscopic substrates. He successfully employed a template-stripping method to produce thick gold surfaces with little roughness. He did measurements for a long range of distances (10 - 1000 nm) in a two cilinders geometry.

Chapter 4

Importance for fundamental force theories

4.1 Introduction

Unified gauge theories, supersymmetry, supergravity and string theory predict that there would exist a number of light and massless elementary particles. Examples of these are the axion, scalar axion, graviphoton, dilaton and arion. When these particles are exchanged between two atoms an interatomic force arises which is described by a Yukawa or power-law effective potential. The force which arises is long-range, from 1 $\mathring{A}$ to cosmic scales. For now it is a hypothetical force. It is often referred to as 'the fifth force' and may be considered as some specific correction to the Newtonian gravitational interactions. Many theories of the standard model exploit the idea of Kaluza-Klein that space-time is not 4-dimensional, but $4 + n$, where the additional n spatial dimensions are compactified at some small length scale. For a long time it was thought that this length scale is in the order of the Planck length, which is 10^{-33} cm. This corresponds to an energy scale of 10^{19} GeV, which is too high to observe directly in an experiment. The more recent models propose a much smaller energy, only 1 TeV. This is the same energy scale as for gauge interactions. Constraints on these new, lower energy scale, compactification models can be obtained by investigating their predictions in accelerator experiments, astrophysics and cosmology.

If one wants to achieve more model independent limits, testing Newtonian gravity is a good way. In exra-dimensional models with large compact extra dimensions, the Newtonian gravitational potential acting between two point masses acquires a Yukawa correction for separations much larger than

the compactification scale. This is a correction of the form $ae^{(r_{12}/\lambda)}$ in which r_{12} is the distance between the masses, a is a dimensionless constant of hypothetical interaction and $\lambda = \hbar/(mc)$ is the interaction range. For models with non-compact but warped extra dimensions, the corrections are power laws. For two interacting macroscopic bodies, either of these corrections would give rise to a new force coexisting with the Newtonian gravitational force and other conventional standard model interactions. Many extensions of the standard model do not involve extra dimensions. These also predict the existence of Yukawa or power-law forces.

Gravitational experiments are done in the range 10^{-2} m $< \lambda < 10^6$ km. They have found no convincing evidence for new forces or extra dimensions. But in the submillimeter range experiments are only possible since a few years. In this range constraints follow from the gravitational experiments and the Newtonian law is not experimentally confirmed.

Around 1997 pioneer studies in applying the Casimir force measurements to the problem of long-range interactions were made. It was shown that in the range 10^{-8} m $< \lambda < 10^{-4}$ m the Casimir effect leads to the strongest constraints on the constants of the Yukawa-type interactions. Nowadays the Casimir effect is a new and powerfull nonaccelerator test for the search of hypothetical forces and associated light and massless elementary particles. These tests are of great importance because they can confirm the new ideas that the gravitational and gauge interactions may become unified at the weak scale. As a consequence, there should exist extra spatial dimensions compactified at a relatively large scale of 10^{-3} m or less. Another consequence is that the Newtonian gravitational law acquires Yukawa-type corrections in the submillimeter range. These were predicted earlier from other considerations. These corrections can be constrained and even discovered in experiments in which precision measurements of the Casimir force are done. These experiments are, in contrast to astrophysical and cosmological constraints, rather model independent, reproducible and therefore more reliable.

4.2 Calculation of constraints

The potential energy between two point masses m_1 and m_2 separated by a distance r is given by the usual Newtonian potential with a Yukawa correction

$$V_r = -\frac{Gm_1m_2}{r}\left(1 + \alpha\exp\left(\frac{-r}{\lambda}\right)\right) \tag{4.1}$$

Here α is a dimensionless constant which characterizes the strength of the Yukawa force and λ is the range of the force. For theories with $n \geq 1$ extra dimensions $\alpha \propto 1$ and $\lambda \propto R_n$, where R_n is the size of the compact dimensions. This equation holds under the condition

$$r >> R_n \propto \frac{1}{M_{Pl}^{(N)}} \left(\frac{M_{Pl}}{M_{Pl}^{(N)}} \right)^{\frac{2}{n}} 10^{\frac{32}{n} - 17} cm \qquad (4.2)$$

Here M_{Pl} is the energy scale corresponding to the planck length λ_{Pl}. Most authors use natural units with $\hbar = c = 1$ so that $M_{Pl} = 1/\lambda_{Pl} = 1/\sqrt{G_N}$ where G_N is the Newtonian gravitational constant. The conversion factor is $\hbar c = 2 \times 10^{-14}$ GeV cm. The relation between the quantities is nicely explained by Milton [17].

For $n = 1$ it follows that $R_1 \propto 10^{15}$ cm. This is excluded by measurements of Newtonian gravity done in the solar system. When $n = 2$ and $n = 3$ the sizes of the extra dimensions are $R_2 \approx 1$ mm and $R_3 \approx 5$ nm, respectively. Recent measurements of gravity in the millimeter distance scales did not lead to evidence for new physics. But gravity remains poorly tested at scales $\leq 10^{-4}$ m. When we consider models of non-compact but warped extra dimensions the potential energy gets a power-law correction given by

$$V(r) = -\frac{G m_1 m_2}{r} \left[1 + \alpha_l \left(\frac{r_0}{r} \right)^{l-1} \right] \qquad (4.3)$$

where α_l is a dimensionless constant, l is a positive integer and $r_0 = 10^{-15}$ m. These forms of corrections can also have another cause, namely the exchange of particles. The Yukawa potential describes forces generated by the exchange of light bosons, such as scalar axions, graviphonons, hyperphotons and dilatons. In this case the interaction constant α can be much larger than unity. Power-law corrections can be due to the simultaeous exchange of two photons or two massless scalars, two massless pseudoscalars, a massless axion or a massless neutrino-antineutrino pair.

The agreement between theory and experiment for Casimir force measurements can be used to set new constraints on the Yukawa strength α as a function of λ from equation 4.1. The total force acting between a sphere and a plate due to this potential is obtained by first integrating over the plate and sphere and then differentiating with respect to z. It can be proved that the contribution of the Newtonian gravitational force is very small and can be neglected [12]. For a Yukawa force the detailed structure of sphere and plate should be considered. In 2003, Decca et al. did Casimir force measurements and used these to get constraints for the Yukawa potential [12]. They

used a sphere with density $\rho_s = 4.1 \times 10^3$ kg/m^3 which was coated with a layer of Cr of thickness $\delta_{Cr} = 1nm$ with $\rho_{Cr} = 7.9 \times 10^3$ kg/m^3 and a layer of Au of thickness $\delta_{Au} = 203$ nm. The plate of density $\rho_{Si} = 2.33 \times 10^3$ kg/m^3 was coated first with the same thickness of Cr and then with a layer of Cu of thickness $\delta_{Cu} = 200$ nm. Provided that the conditions $z, \lambda << R, D$ are satisfied, which is the case in this experiment, the hypothetical force is given by

$$
\begin{aligned}
F^{hyp}(z) &= -4\pi^2 G\alpha\lambda^3 \exp\left(-z/\lambda\right) R[\rho_{Au} - (\rho_{Au} - \rho_{Cr})\exp\left(-\Delta_{Au}/\lambda\right) \\
&\quad - (\rho_{Cr} - \rho_s)\exp(-(\Delta_{Au} + \Delta_{Cr})/\lambda)] \\
&\quad \times [\rho_{Cu} - (\rho_{Cu} - \rho_{Cr})\exp(-\Delta_{Cu}/\lambda) \\
&\quad - (\rho_{Cr} - \rho_{Si})\exp(-(\Delta_{Cu} + \Delta_{Cr}/\lambda)]
\end{aligned}
\tag{4.4}
$$

In this experiment the Casimir force is measured dynamically and statically. The strongest constraints come from the dynamical measurements of the parallel plate pressure, which is the Casimir force gradient. The Yukawa pressure can be calculated by using the PFA, which says that

$$
-\frac{\delta F_C(z)}{\delta z} = 2\pi R P_C(z)
\tag{4.5}
$$

where $P_C(z)$ is the force per unit area between two infinite plates. The Yukawa pressure is thus given by

$$
\begin{aligned}
P^{hyp}(z) &= -2\pi^2 G\alpha\lambda^2 \exp(-z/\lambda)[\rho_{Au} - (\rho_{Au} - \rho_{Cr})\exp\left(-\Delta_{Au}/\lambda\right) \\
&\quad - (\rho_{Cr} - \rho_s)\exp(-(\Delta_{Au} + \Delta_{Cr})/\lambda)] \\
&\quad \times [\rho_{Cu} - (\rho_{Cu} - \rho_{Cr})\exp(-\Delta_{Cu}/\lambda) \\
&\quad - (\rho_{Cr} - \rho_{Si})\exp(-(\Delta_{Cu} + \delta_{Cr}/\lambda)]
\end{aligned}
\tag{4.6}
$$

Surface roughness should be taken into account, since it can significantly influence the magnitude of a hypothetical force in the nanometer range, as was described in chapter 3. The correction factor Decca uses is

$$
P_R^{hyp}(z) = \sum_{i,j=1}^{n} v_i v_j P^{hyp}\left(z + 2H_0 - h_i - h_j\right)
\tag{4.7}
$$

Here v_i is the surface area and h_i is the height of this area. H_0 is the zero roughness level and z is the distance between the plates.

This result can be used to obtain the desired constraints on the hypothetical Yukawa pressure. In this experiment, the optimal separation region

for obtaining constraints turned out to be $z > 310$ nm. Using only this region leads to a smaller rms deviation, $\sigma_{1100} + P$, between theory and experiment. Within the choosen interval, the strongest constraints are obtained for the shortest distances. $z_0 = 320$ nm is choosen and constraints are obtained from the inequality

$$|P_R^{hyp}(z_0)| \leq \sigma_{1100} + P = 0.34mPa \tag{4.8}$$

The constraints are plotted in figure 4.1 for different values of the interaction range λ (curve 1). In the same figure constraints from previous experiments are shown. They were obtained from old measurements of the Casimir force between dielectrics (curve 2), from Casimir force measurements by means of a torsion pendulum (curve 3) and by the use of an AFM (curve 4). In all cases the region in the (α, λ)-plane above the curve is excluded and below the curve is allowed by the experimental results. From this figure we can see that the present experiment leads to the strongest constraints in a wide interaction range, 56 nm $\leq \lambda \leq$ 330 nm. The largest improvement, by a factor of 11, is achieved at $\lambda \approx 150$ nm. The measurements of Decca *et al.* [12] fill the gap between the modern constraints obtained by AFM measurements, and those using a torsion pendulum. Before, the best constraints in this range were obtained from old measurements of the Casimir force between dielectrics, which are less precise and reliable.

For the power-law-type hypothetical interactions the present experiment does not lead to improved constraints. This is because the metallic coatings used were too thin and hence to light to give a significant contribution to the hypothetical interactions with a longer interaction range. The thicker bulk matter contributes more significantly in this case, even though its density is much lower than for metal coatings. Therefore, in order to obtain stronger constraints for the power-law interactions, thicker metal coatings and larger interacting bodies are nessecary.
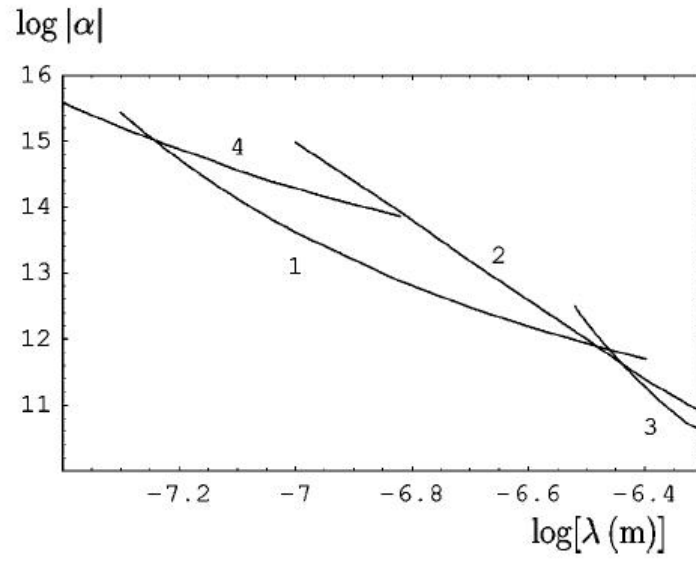
Figure 4.1: Constraints on the Yukawa interaction constant α versus interaction range λ. The region in the (α, λ)-plane above each curve is excluded and below each curve is allowed.

Chapter 5

Effect of the Casimir force in small systems

5.1 Introduction

These days the ultimate goal in the field of electronics is the realization of atom-level information storage, computing, signal processing and mechanical functions. Furthermore, the emergence of new materials, concepts and techniques has opened up new possibilities to implement new electronics technology with attributes that are far superior to everything known to date. At such small length scales, physical properties and effects, for instance electronic, mechanical, optical and magnetic and quantum effects are yet mostly unknown.

Because the silicon infrastructure is very good and huge investments have been made herein, one tries to capture the new opportunities while inducing a minimum of process disruption. One of the novel fields is that of the nano electromechanical systems (NEMS) and micro electromechanical systems (MEMS). It derives from exploiting progress in techniques for the the fabrication, down to nanometer length scales, of device structures that incorporate mechanical motion and that may be designed to perform a variety of functions. These can be optical, electrical and mechanical or mixed domain. It exploites the wave nature of electrons, but also novel quantum mechanical effects such as quantized heat flow, manifestation of charge discreteness, and the quantum electrodynamical Casimir effect. In this regime, new device circuit paradigms must be invoked in order to fully exploit the potential of this technology in computation and signal processing applications.
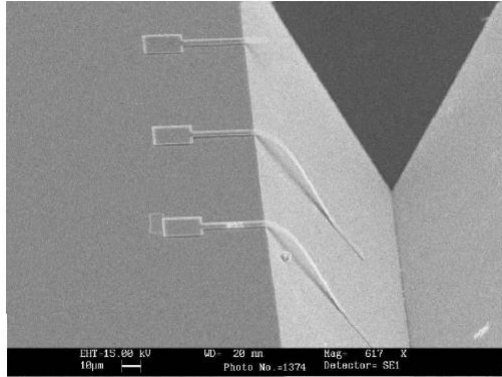
Figure 5.1: Stiction of microcantilevers to substrate. (Picture taken from [18]).

One of the fundamental issues in building MEMS or NEMS is the scale effect. The surface-to-volume ratio increases when the dimensions of the device decrease. Therefore, the types of forces that influence microscale devices are different from those that influence devices with conventional scale. The surface effect induces strong adhesion, friction and wear. These are major problems limiting both the fabrication yield and operation lifetime of many MEMS and NEMS devices. Strong adhesion is generally caused by capillary, electrostatic, or van der Waals forces, and other kind of chemical forces. Stiction is the unintentional adhesion of compliant microstructure surfaces when restoring forces are unable to overcome interfacial forces. For MEMS and NEMS there are two categories. Release-related stiction, which occurs during the sacrificial layer removal process in fabrication of microstructures, is primarily caused by capillary forces. In-use stiction usually occurs upon exposure of succesfully released microstructures to a humid environment. An example of stiction is given in figure 5.1. Adhesion (stiction) failure is one of the most important issues concerning reliabilityof MEMS and NEMS.

5.2   Fabrication of NEMS

Mechanical structures require the incorporation of techniques to shape the dimension normal to the wafer. This is in contrast to molecular and meso-scopic devices, whose physical embodiment is made by electron-beam lithography or photo-beam lithography or chemical etching and have a succession of two dimensional layout patterns on a wafer surface. There are different

techniques to do this [11]:

- scanning probe approaches, in which use is made of scanning tunneling and atomic force microscopes (AFM's) to effect direct manipulation of the particles forming the device structures themselves;

- soft lithography approaches, in which mechanical processes, such as contact printing and molding are utilized to transfer onto a wafer the pattern of previously prepared nanoscale elastic mold;

- self-assembly approaches, in which chemical reactions are engineered to coerce the assembly of atoms and molecules into forming the desired nanostructures.

These approaches are promising, but they are still in a developmental stage. It is possible to create precise nanostructures via these emerging techniques. The drawbacks are that they are too slow for large volume manufacturing, inadequate for creating multilayer structures, and ill-suited for producing complex arrays of interconnected devices. That is why mostly derivatives of the well established approaches for creating MEMS are used to make NEMS. These are surface micromachining and bulk micromachining.

In surface micromachining thin-film materials are selectively added to and removed from the wafer. The film materials that are eventually removed are called sacrificial materials and those that remain are called structural materials. In bulk micromachining mechanical structures are created witin the confines of the silicon wafer. First a wafer pattern is made using electron-beam lithography. Then, wafer material is selectively removed by wet and dry etching techniques. Thus use is made of the anisotropic etching rates of the different crystal planes in the wafer.

5.3 Adhesion at microscales

Early experiments with a soft rubber sphere in contact with glass showed that the relative magnitude of the adhesion varies inversely with the product of the contact size and the equivalent elastic modulus of the two surfaces. To get a better understanding of adhesion between solid-solid surfaces we have to take into account the surface roughness. A studie of adhesion will be described, following [18].

To study the adhesion of movable MEMS to the substrate, a dimensionless number, the peel number N_p, is defined. It is the ratio of elastic strain
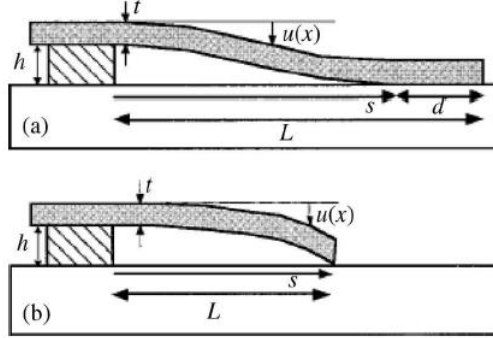
Figure 5.2: Above: S-shaped cantilever adhered to the substrate over a distance d. Below: arc-shaped cantilever adhered to the substrate onl very near its tip. (Picture taken from [18]).

energy stored in the deformed microstructure to the work of adhesion between the microstructure and the substrate. If $N_p \geq 1$, the restored elastic strain energy is greater than the work of adhesion and the microstructure will not adhere to the substrate. If, on the other hand, $N_p \leq 1$, the deformed microstructure does not have enough energy to overcome the adhesion between the beam and the substrate.

For a long slender cantilever of thickness t and elastic modulus E suspended at a distance h from the substrate, as illustrated in fig 5.2, the peel number is

$$N_p = \frac{3Et^3h^2}{2s^4W_a} \tag{5.1}$$

where s is the crack length and W_a is the work of adhesion between the cantilever and the substrate. For a short cantilever beam with just its tip adhered to the substrate as is also shown in figure 5.2, the corresponding peel number is

$$N_p = \frac{3Et^3h^2}{8L^4W_a} \tag{5.2}$$

The maximum dimensions of the microstructure that will not stick to the substrate can be obtained from the last equation. In this simplest case this length is the length of the cantilever. Formulas for the width of a square plate and the radius of a circular plate are given in [18].

Zhao *et al.* [18] show that the effective adhesion W_c when the surface roughness is taken into account is given by

$$W_c = f(\theta)W_a \tag{5.3}$$

where

$$f(\theta) = C \int_{s_e}^{\infty} Y_\theta ds \tag{5.4}$$

where

$$Y_\theta = \frac{4\theta}{3\sqrt{2\pi}} \int_s^{\infty} (x-s)^{\frac{3}{2}} \exp\left(-\frac{x^2}{2}\right) dx - \sqrt{2\pi} \int_s^{\infty} \exp\left(-\frac{x^2}{2}\right) dx \tag{5.5}$$

is a dimensionless roughness function reflecting the influence of surface roughness on adhesion. Here $s = \frac{d}{\sigma}$ and $x = \frac{z}{\sigma}$ with $\sigma =$ the standard deviation of a gaussian distribution, are dimensionless parameters, θ is the roughness parameter and s_e is the equilibrium separation.

In the case of an S-shaped cantilever beam with a rough substrate the detachment energy of the cantilever from the substrate is

$$U_s = w\left(L-s\right)W_c = w\left(L-S\right)f(\theta)W_a \tag{5.6}$$

and the elastic strain energy is

$$U_E = \frac{EI}{2} \int_0^s \left(\frac{d^2u}{dx^2}\right)^2 dx = \frac{6EIh^2}{s^3}. \tag{5.7}$$

The corresponding peel number for cantilever beam adhesion to a rough surface is determined by the equilibrium condition

$$\frac{d\left(U_s + U_E\right)}{ds} = 0 \tag{5.8}$$

from which follows that

$$N_P^r = \frac{N_P}{f(\theta)} \tag{5.9}$$

where N_P is the peel number for smooth contact and N_P^r is the peel number considering rough contact. As we can see the adhesion of a cantilever beam with a rough substrate is reduced with increasing adhesion parameter θ.

In this derivation it is assumed that the height distributions are Gaussian, which is too restrictive for many important applications. For models of fractal surfaces see [18].

5.4   Adhesion by the Casimir force

In MEMS and NEMS a lot of interesting phenomena occur, such as the manifestation of charge discreteness, quantized heat flow and the quantum electrodynamic Casimir effect. Here only the last one will be discussed, a discussion of the other phenomena can be found in [11]. The Casimir force is important for NEMS and MEMS because it predicts a force between macroscopic bodies, although the origin is quantum mechanical. The Casimir force thus influences the performance and yield of these devices. It has been associated with the van der Waals force, which also acts at small length scales. The van der Waals force is of electromagnetic and quantum mechanical origin, and is responsible for intermolecular attraction and repulsion. In general the Casimir force is dominant at a slightly longer length scale. As we saw in the introduction, the Casimir force between two parallel uncharged plates in vacuum is given by

$$F(a) = -\frac{\pi^2}{240}\frac{\hbar c}{a^4}S \qquad (5.10)$$

where $S >> a^2$ is the area of the plates. For an area $S = 1$ cm^2 and separation distance $a = 0.5\mu$m the Casimir force is 2×10^{-6} N. In practical applications, it is seen that at distances less than 100 nm the movable components in NEMS and MEMS often stick together due to the Casimir force.

5.5   Casimir effect oscillator

The new electronics enabled by NEMS operate in the quantum mechanical regime. Thus, the phenomena that occur, under which the Casimir effect, can be exploited to create powerful computing and communications hardware. One of the devices that makes use of this effect is the Casimir effect oscillator. It was proposed and analyzed by Serry [19] in 1995 and experimentally realized by Chan [14] in 2001. It is the first clear demonstration of the impact of the Casimir force in the performance of a NEM. In the experiment, the proximity of a vibrating rotational resonator to a metallic sphere was changed in order to measure its behaviour in the absence and presence of the Casimir force. The setup is shown in figure 5.3. First the drive for linear response is determined, then the proximity of the oscillator to a metallic sphere is varied and the resonance frequency is measured. It behaves as in figure 5.4. For sphere-oscillator distances greater than 3.3μm, the oscillator frequency was equal to the drive frequency, 2748 Hz, and the angular amplitude frequency response was symmetric and centered on the drive frequency

$$F_{Spring} = kz \qquad F_{Casimir} = \frac{\pi^3 \hbar c}{120} \frac{R}{z^4}$$

$$V_{Spring}(z) = \frac{1}{2} \left(\frac{z}{z_{max}} \right)^2 \qquad V_{Casimir}(z) = \frac{C}{\left(1 - \dfrac{z}{z_{max}} \right)^3}$$
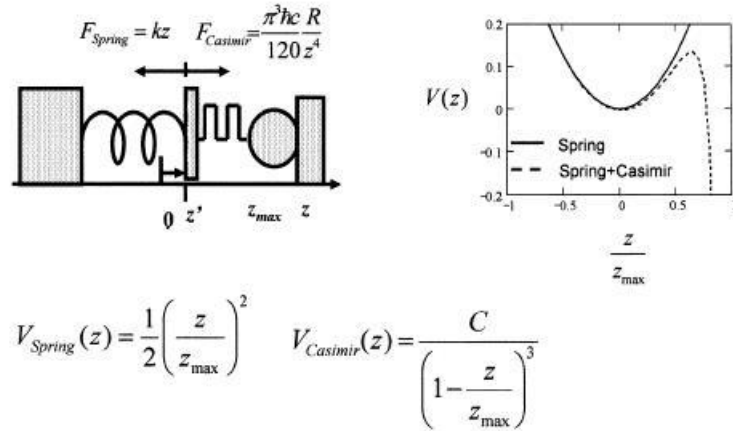
Figure 5.3: Summary of the nonlinear Casimir effect MEM resonator physics. (This picture and next taken from [11]).
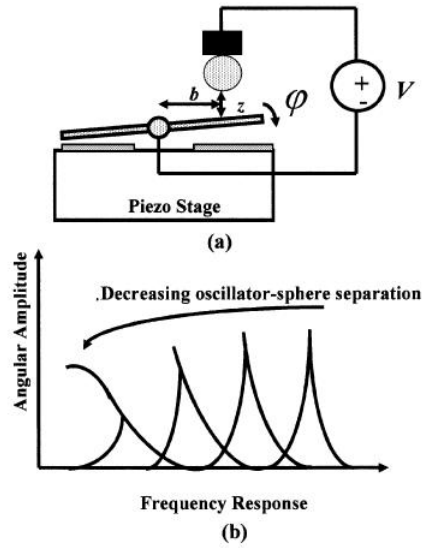

Figure 5.4: Schematic picture of torsional MEM oscillator and sketch of the Casimir effect on the resonance response.

$\omega_0 = \sqrt{k/I}$ where k is the spring constant, and I the moment of inertia. This is consistent with mass-spring force oscillator behaviour. As the sphere-oscillator distance is decreased, the resonance frequency shifts according to $\omega_1 = \omega_0[1 - b^2 F'(z)/2I\omega_0^2]$ where b is the lateral distance of the sphere from the center of the top plate, F_z' is the first derivative of the external force evaluated at z, and the angular amplitude frequency response asymmetric and hysteretic. This behaviour is consistent with the dynamics of a mass-spring-Casimir force system. This experiment has had a great impact, in particular it showd that the Casimir force will be one of the factors limiting the integration level or density of NEMS and MEMS.

Chapter 6

Improvements and prospects

Nowadays, researchers have developed sensitive force detection techniques such as phase sensitive detection and the scanning probe microscope. Forces between 10 and 1000 nm can be measured. Of course this region should be broadened, especially to smaller distances. This is necessary to put stronger constraints on the formulas for the compactified dimensions as postulated by modern unified theories. The Casimir force above separations of 1 μm is also of great interest as a test for some predictions of supersymmetry and string theory. To measure at smaller distances, smoother metal coatings should be used. This can be realized by atomic layer by layer growth or molecular beam epitaxy. Even with these methods there will still be single atomic steps of ≈ 0.5 nm, so the smallest separation distance that can possibly be achieved is on the order of 1-2 nm.

Of course the measurements of the Casimir force should be reproducible, which means that all the parameters, like surface separation, electrostatic forces between surfaces, and surface roughness, should be determined independently. One also needs to measure the errors introduced due to the uncertainties in the measurements of these factors.

The theory of how finite surface conductivity, finite temperature and rough surfaces can be taken into account needs further development. Now a rather simple expression is known, but this one only holds for an accuracy of $< 1\%$. Models need to be developed which can take into account these factors with much higher accuracy.

It is anticipated that the strength of the constraints on the constants of hypothetical long-range interactions obtained by means of the Casimir effect will be increased at least by four orders of magnitude in the next few years. When this is done, it will be possible to check the Newtonian gravitational

law in the submillimeter range which was not possible by other methods the last 300 years. From this the exceptional predictions concerning the structure of space-time at short scales can be confirmed or rejected by the measurement of the Casimir force.

Before nanodevices can be used to help mankind, the laws they obey should be fully understood. Two main challenges arise. The first one is communication between the nanoworld and the macroworld, which is difficult because all measurable quantities are very small at these scales. The second one is the increasingly dominant surface when devices become smaller. Much of the foundation of solid state physics lies on the assumption that the surface-to-volume ratio is infinitesimal, which means that physical properties are always dominated by the properties of the bulk. For nanodevices this assumption breaks down completely.

Concluding, a lot of work has been done in this field, and still a lot more remains to be done in order to fully understand and exploit the usefull aspects of the Casimir force.

Chapter 7

References

Articles referred to in the text

1. *Effet Casimir et interaction entre plasmons de surface*, F. Intravia, Université Pierre et Marie Curie

2. *New developments in the Casimir effect*, M. Bordag, U. Mohideen, V.M. Mostepanenko, Physics Reports 353 (2001) 1-205

3. *The influence of retardation on the London-van der Waals forces*, H.B.G. Casimir, D. Polder, Physical Review 73-4 (1948)

4. *Temperature dependence of atom-atom interactions*, H. Wennerström, J, Daicic, B.W. Ninham, Physical Review A 60-3 (1999)

5. *Attractive Casimir forces in a closed geometry*, M.P. Hertzberg, R.L. Jaffe, M. Kardag, A. Scardicchio, 2006

6. M.J. Sparnaay, physica 24 (1958) 751.***

7. *Temperature dependence of the Casimir effect between metallic mirrors*, C. Genet, A. Lambrecht, S. Reynaud, Physical Review A 62 012110 (2000)

8. V.B. Bezerra, G.L. Klimchitskaya, C. Romero, Mod. Phys. Lett. A 12, 2613 (1997); A.A. Maradudin, P. Mazur, Phys. Rev. B 22, 1677 (1980)

9. *Casimir effect with rough metallic mirrors*, Paulo A. Maia Neto, A. Lambrecht, S. Reynaud, Physical Review A, 72 012115 (2005)

10. *Influence of finite sample conductivity on phase maps of microelectromechanical switches in the presence of the Casimir force*, G. Palasantzas, J.Th.M. De Hosson (2005)

11. *Nanoelectromechanical quantum circuits and systems*, Hector J. De los Santos, invited paper

12. *Improved tests of extra-dimensional physics and thermal quantum field thory from new Casimir force measurements*, R.S. Decca, E. Fischbach, G.L. Klimchitskaya, D.E. Krause, D. Lopez, V.M. Mostepanenko, Physical Review D 68 116003 (2003)

13. *Measurement of the Casimir force between parallel metallic surfaces*, G. Bressi, G. Carugno, R. Onofrio, G. Ruoso, Physical Review Letters 88.041804 (2002)

14. *Nonlinear micromechanical Casimir oscillations*, H.B. Chan, V.A. Aksyuk, R.N. Kleiman, D.J. Bishop, F. Capasso, Physical Review Letters 87.2111801 (2001)

15. *Demonstration of the Casimir force in the 0.6 to 6 µm range*, S.K. Lamoreaux, Physical Review Letters 78 number 1 (1997)

16. *Novel surfaces for force measurements* WITH APPLICATIONS TO FUNDAMENTAL PHENOMENA, T. Ederth, Stockholm, ISBN 91-7170-448-5

17. *The Casimir effect: Recent controversies and progress*, K.A. Milton, PACS numbers: 11.10.Gh, 11.10.Wx, 42.50.Pq, 78.20.Ci

18. *Mechanics of adhesion in MEMS - a review*, Y.P. Zhao, L.S. Wang, T.X Yu, J. Adhesion Sci Technol. Vol 17 No 4, pp. 519-546 (2003)

19. *The anharmonic Casimir oscillator (ACO) - the Casimir effect in a model microelectromechanical system*, F.M. Serry, D. Walliser, G.J. Maclay, J. Microelectromech. Syst. vol 4 pp. 193-205, (1995)

20. *Theory of the stability of lyophobic colloids*, E.J.W. Verwey, T.G. Overbeek, K. van Nes, Elsevier publishing compagny, Inc. Amsterdam

Other articles used

1. *The Casimir effect: a force from nothing*, A. Lambrecht, http://physicsweb.org/articles/world/15/9/6

2. *Casimir effect: experiment-theory comparison*, F. Intravia, A. Lambrecht, S. Reynaud, Laboratiore Kastler-Brossel, UPMC-ENS-CNRS, 4 place Jussieu, F-75252 Paris

3. *Nanocase presentation*, C. Binns, A. Lambrecht, B. Sernelius, M. Ward

4. *Micromechanics and measurements of interactions at nanoscale*, J. Chevrier, Phd thesis

5. *FOM handwijzer*, PR 2005

6. *Stiction, adhesion energy and the Casimir effect in micromechanical systems*, E. Buks, M.L. Roukes, Physical review B, vol. 63, 033402 (2001)

7. *Precision measurements of the Casimir force using gold surfaces*, B.W. Harris, F. Chen, U. Mohideen, Physical review A, vol. 62, 052109 (2000)

8. *Plenty of room, indeed*, M. Roukes, Scientific American, (september 2001)